Performance of Thin Piezoelectric Materials for Pyroelectric Energy Harvesting

J. Xie, X.P. Mane, C.W. Green, K.M. Mossi and Kam K. Leang

Journal of Intelligent Material Systems and Structures 2010 21: 243 originally published online 11 November 2009
DOI: 10.1177/1045389X09352818

Performance of Thin Piezoelectric Materials for Pyroelectric Energy Harvesting

J. XIE,[1] X. P. MANE,[1] C. W. GREEN,[1] K. M. MOSSI[1,*] AND KAM K. LEANG[2,*]

[1]*Department of Mechanical Engineering, Virginia Commonwealth University, Richmond, VA 23284, USA*

[2]*Department of Mechanical Engineering, University of Nevada - Reno, Reno, NV 89557, USA*

ABSTRACT: This article considers pyroelectric energy harvesting using piezoelectric materials such as PZT-5A, PMN-PT, PVDF, and thin-films. A model is developed to predict the power generation based on the temporal change in temperature of the material. The measured and predicted power measurements are compared, where the maximum power density of $0.36\,\mu W/cm^2$ is calculated with PMN-PT. The predicted peak power density under similar boundary conditions for thin-film lead scandium tantalate is over $125\,\mu W/cm^2$. The study concludes that the power density is highly dependent upon the surface area and the pyroelectric coefficient of the material, underlining the importance of maximizing these parameters.

Key Words: piezoelectric materials, pyroelectric energy harvesting, power density.

INTRODUCTION

DUE to recent advances in low-power portable electronics and the fact that batteries in general provide a finite amount of power, attention has been given to explore methods for energy harvesting and scavenging. Energy can be recovered from mechanical vibrations (Sodano et al., 2004; Mossi et al., 2005), light, and spatial and temporal temperature variations (Roundy et al., 2003; Paradiso and Starner, 2005).

Thermal energy in the environment is a potential source of energy for low-power electronics. For example, a recent commercial product, a wristwatch, uses thermoelectric modules to generate enough power to run the clock's mechanical components (Paradiso and Starner, 2005). The thermoelectric modules in the clock work on the thermal gradient provided by body heat. Similar modules can be used for powering low-power sensors used in structural health monitoring systems.

Ferromagnetic materials have been exploited to convert thermal into electrical energy (Ujihara et al., 2007). In this sense, they are attractive for recycling wasted heat into useable energy, and they can be used to create highly reliable, silent, and environmentally friendly energy harvestors (Rowe, 1995, 1999; Wu, 1996). A recent patent was issued for energy harvesting using novel thermoelectric materials (Nersessian et al., 2008), and also research has shown that batteries can be recharged using thermal gradients (Sodano et al., 2007). One of the challenges of thermoelectric materials for energy harvesting is the need for spatial temperature gradients.

The pyroelectric effect is another possibility for directly converting heat into electricity. Rather than harvesting energy from spatial temperature gradients, pyroelectric materials produce power from temporal temperature changes (Whatmore, 1986). In particular, charge is produced when the material's temperature is altered as a function of time; likewise, a change in temperature results in mechanical deformation. In the past few years considerable amount of research has been conducted on using PZT pyroelectric materials for energy harvesting and storage (Borisenok et al., 1996; Bauer, 2006; Cuadras et al., 2006). Several factors must be considered to optimize the performance of such materials for a given application. For example, the material's geometry, the boundary conditions, and even the circuitry used to harvest power must be carefully considered (Sebald et al., 2008; Guyomar et al., 2009). The contributions of this work include investigating the potential application of thin pyroelectric materials for energy harvesting and examining the important parameters that affect power generation.

One approach to enhance energy generation is to use pyroelectric materials with significantly higher pyroelectric coefficients. A recent study showed that thin films with volume fractions similar to bulk PZT exhibit orders of magnitude higher pyroelectric coefficients (Lam et al., 2004). In the following, a model is developed to predict the power generated based on the temperature of a

*Authors to whom correspondence should be addressed.
E-mail: kmmossi@vcu.edu and kam@unr.edu
Figures 2, 3 and 7 appear in color online: http://jim.sagepub.com

1045-389X/10/03 0243–7 $10.00/0 DOI: 10.1177/1045389X09352818

pyroelectric material. The model is validated experimentally using PZT-5A, PMN-PT, and PVDF samples. The model is also used to predict power generation for other pyroelectric materials with higher pyroelectric coefficients, such as thin-film lead scandium tantalite (Watton and Todd, 1991; Todd et al., 1999) and lead magnesium niobate lead titanate (Kumar et al., 2004; Sebald et al., 2008).

MODELING

A material is considered to exhibit the pyroelectric effect when a change in the material's temperature with respect to time (temporal change) results in the production of electric charge (Whatmore, 1986; Bauer, 2006). Specifically, the detectable current $i_p(t)$ of a pyroelectric material is proportional to the rate of change of its temperature (Whatmore, 1986), i.e.,

$$i_p(t) = p' A \frac{\mathrm{d}T(t)}{\mathrm{d}t}, \tag{1}$$

where p' is the component of the pyroelectric coefficient vector p orthogonal to the electrode surface of area A; and $T(t)$ denotes the temperature with respect to time. For convenience, the heating and cooling behavior of the material is not considered.

A lumped-parameter model of a pyroelectric element is shown in Figure 1. The pyroelectric element is modeled as a current source $i_p(t)$ in parallel with an internal capacitance C_p. The figure also shows the pyroelectric element connected in parallel with an external capacitor C_e and resistor R_e. The objective is to determine the element's output voltage $V_p(t)$ and power $P(t)$ generated for a given temperature profile $T(t)$.

For a given temperature profile $T(t)$, the instantaneous power dissipated by the resistor R_e can be determined with knowledge of the output voltage $V_p(t)$:

$$P(t) = \frac{V_p^2(t)}{R_e}. \tag{2}$$

On the other hand, the generated power can be predicted using Equation (1) as follows. Assuming zero initial conditions, summing currents in the circuit shown in Figure 1, the following relationship is obtained:

$$p' A s T(s) = C s V_p(s) + \frac{1}{R_e} V_p(s), \tag{3}$$

where s is the Laplace variable and $T(s)$ and $V_p(s)$ are the Laplace transforms of the input temperature and output voltage, respectively. The total capacitance C is the sum of internal capacitance, C_p and the external capacitance, C_e. Therefore, the transfer function relating the input temperature $T(s)$ to the output voltage $V_p(s)$ is:

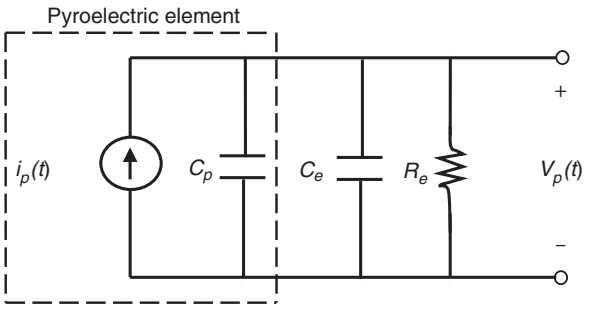

Figure 1. *A lumped-parameter model of a pyroelectric element, which is modeled as a current source $i_p(t)$ in parallel with an internal capacitance C_p, connected in parallel to an external capacitor C_e and resistor R_e. The current $i_p(t)$ is proportional to the rate of change of temperature of the device. The voltage generated by the pyroelectric element is denoted by $V_p(t)$.*

$$G(s) \triangleq \frac{V_p(s)}{T(s)} = \frac{p' A s}{C s + 1/R_e}. \tag{4}$$

For a given temperature profile $T(t)$, the generated output voltage $V_p(t)$ across the pyroelectric element can be predicted by using Equation (4). Then, the power dissipated across the resistor can be calculated using Equation (2). The thermal dynamic effects such as the heating and cooling rate of the pyroelectric element are not captured in the above expression, Equation (4).

THE EXPERIMENTAL SYSTEM

The above model was compared to experimentally obtained power measurements. The experiments were conducted using PZT type OPT 5100 purchased from Omega Piezoceramics Inc., PMN-PT type TRS-X2A from TRS ceramics, and PVDF film from Measurement Specialties, Inc. with relevant properties listed in Table 1.

The experimental system is shown in Figure 2, where the thin sample element was bonded to a thin resistance heater (Minco HK5578 R35.0L12B, 1.91 cm × 1.91 cm). The assembly was subjected to the ambient temperature and not in contact with any surfaces. The heater was used to control the temperature of the pyroelectric element and a Type K thermocouple sensor was attached to the backside of the resistance heater to measure the temperature of the heater. The measured temperature was assumed to be the temperature of the sample. The thermocouple sensor output was connected to an Analog Devices AD595 monolithic thermocouple amplifier and the signal was recorded using a data acquisition system (National Instruments, LabPC+, 12-bit).

The block diagram of the system used to control the temperature of the heater is shown in Figure 3(a).

Table 1. Material properties.

Sample	Thickness (μm)	Area (cm^2)	Pyroelectric coefficient ($\mu C/m^2/K$)	Capacitance (nF)	Curie temperature (°C)
PZT-5A	150	1.44	238[a]	45[a]	350[c]
PMN-PT	273	0.98	416[a]	15[a]	150[c]
PVDF	110	1.96	9[b]	0.090[a]	165[4]

[a]Measured, [b]Malmonge et al. (2003), [c]APC Inc. (2002), [d]Teyssedre et al. (1995).

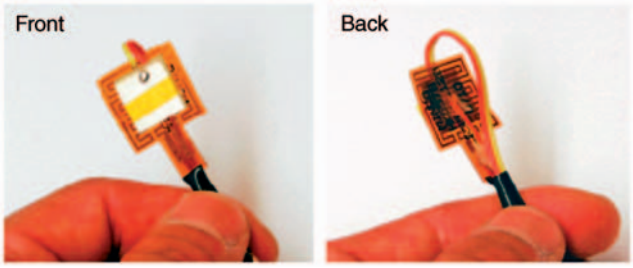

Figure 2. *Photographs of front and back view of the PZT-5A sample mounted to a thin-film resistance heater (Minco HK5578 R35.0L 12B). The thermocouple temperature sensor is fixed to the backside of the heater.*

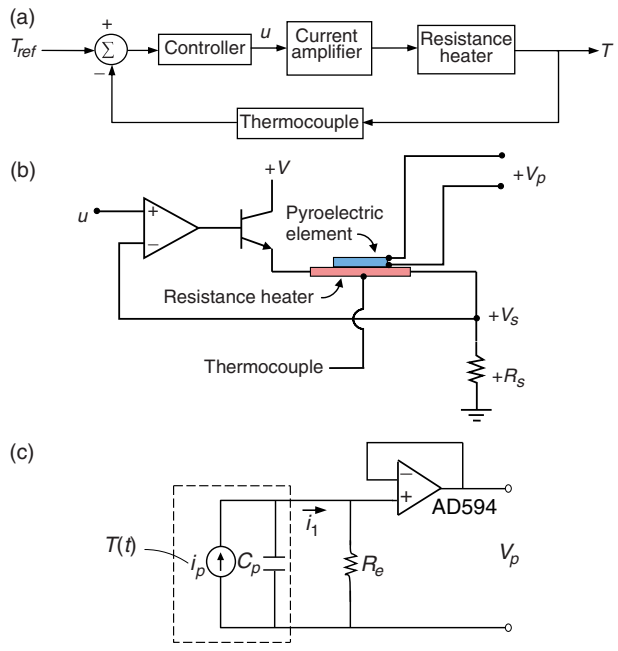

Figure 3. *The experimental setup: (a) the block diagram of the temperature control system: (b) a schematic of the current amplifier, resistance heater, and thermocouple system; and (c) the circuit diagram for measuring generated power. The AD549 was used to isolate the experimental setup from measurement system.*

The current amplifier circuit for the resistance heater is shown in Figure 3(b). The peak heating rates were set according to the operating temperature ranges of the elements being tested. Finally, the circuit diagram for measuring the generated voltage across the resistor R_e is shown in Figure 3(c). As an illustrative example, the external capacitance and resistance were chosen as $C_e = 0$ and $R_e = 1\,M\Omega$, respectively. The chosen resistor value was not optimized for maximum power generation.

THE MEASURED AND PREDICTED RESULTS

The temperature control system was tuned to achieve a relatively high temperature rate, which was slightly different for each element depending on their properties and the ambient temperature. The average heating rate between all of samples was 16.6°C/s.

In case of the PZT, a temperature range of 29.79–102.78°C was used for the experiments, achieving a peak heating rate of 15.65°C/s (Figure 4(a)). The resulting measured and predicted output voltage profiles V_p for the PZT-5A element are shown in Figure 4(b). As seen in the graph, both the profiles are in good agreement. Similarly, the profiles for power are also compared as shown in Figure 4(c). Like the voltage results, the measured and predicted calculated dissipated powers are in good agreement, taking on values of 0.28 and 0.33 μW, respectively. The power densities were determined by normalizing the power measurements with the sample area given in Table 1. The peak power densities for the numerical and experimental results were 0.23 and 0.20 $\mu W/cm^2$, respectively.

Similarly, experiments and simulations were conducted with a PMN-PT sample where the results are shown in Figure 5(a)–(c). The temperature range was from 22°C to 103.9°C, achieving a heating rate of 14.45°C/s as shown in Figure 5(a). The measured and predicted peak voltages were 0.57 and 0.59 V, respectively, as shown in Figure 5(b). Not only does the experimentally obtained power closely follow the predicted profile (Figure 5(c)), but also the peak power values are in good agreement at 0.33 and 0.35 μW. Similar to the case of PZT, power densities were determined for PMN-PT with the measured and predicted results of 0.33 and 0.36 $\mu W/cm^2$, respectively. In all cases the differences between the predicted and measured results were less than 10%.

Results for the third material tested, PVDF, are shown in Figure 6(a)–(c). Temperatures in this case ranged between 30°C and 141°C with a resultant heating rate of 19.64°C/s as shown in Figure 6(a). Peak voltages

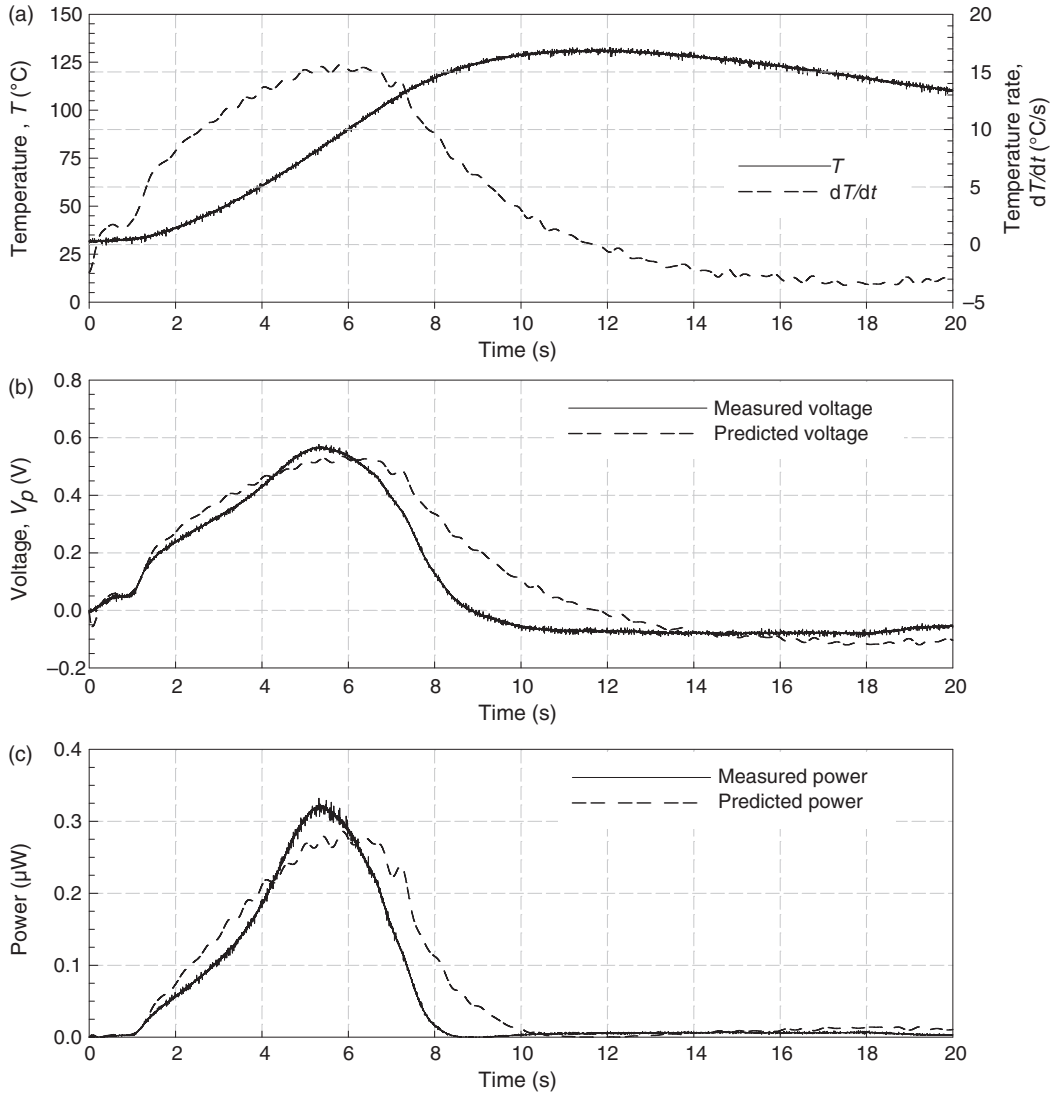

Figure 4. *Measured and predicted results of power generated by PZT-5A element: (a) temperature and temperature rate (*dT/dt*) vs time; (b) measured and predicted PZT voltage vs time; and (c) Measured and predicted power vs time.*

of 0.49 and 0.51 V were obtained experimentally and numerically (Figure 6(b)). The power profile are shown in Figure 6(c) resulting in maximum power of 0.24 and 0.26 μW and power densities of 0.12 and 0.13 $\mu W/cm^2$ for calculated and predicted values, respectively.

All the results are summarized in Table 2. As evident in the table the best match, with the smallest difference between measured and predicted results, is seen in the case of the PMN-PT samples, followed by PVDF and PZT samples. Differences in the voltage readings of only 4% are seen for the PMN-PT samples. Also the largest power generated is with PMN-PT even though it has a comparatively smaller area. This can be explained by its significantly larger pyroelectric coefficient. With dimensions similar to the PMN-PT sample used in the experiments, the power density for a lead scandium tantalite (PST) sample with pyroelectric coefficient $p' = 6000\,\mu C/m^2/K$ is predicted to be 125 $\mu W/cm^2$, which is approximately three orders of larger magnitude. Another enhancing factor could be its large thickness, although it is not included in the model calculations. Thickness could indirectly affect the temperature gradient, thus affecting the power generation. Since the PMN-PT sample was comparatively much thicker than the rest of the materials (82% more than PZT), a peak temperature of 103°C could be used safely in spite of having a low transition temperature of 80°C without damaging the sample. Following PMN-PT, the next largest power density was with PZT, then with PVDF. This trend was expected because of the ordering of the pyroelectric coefficient. While comparing with another energy harvesting source such as mechanical vibrations the energy densities generated by PZT energy harvesting are much higher, 32 mW/cm^2 (Lu et al., 2004) and

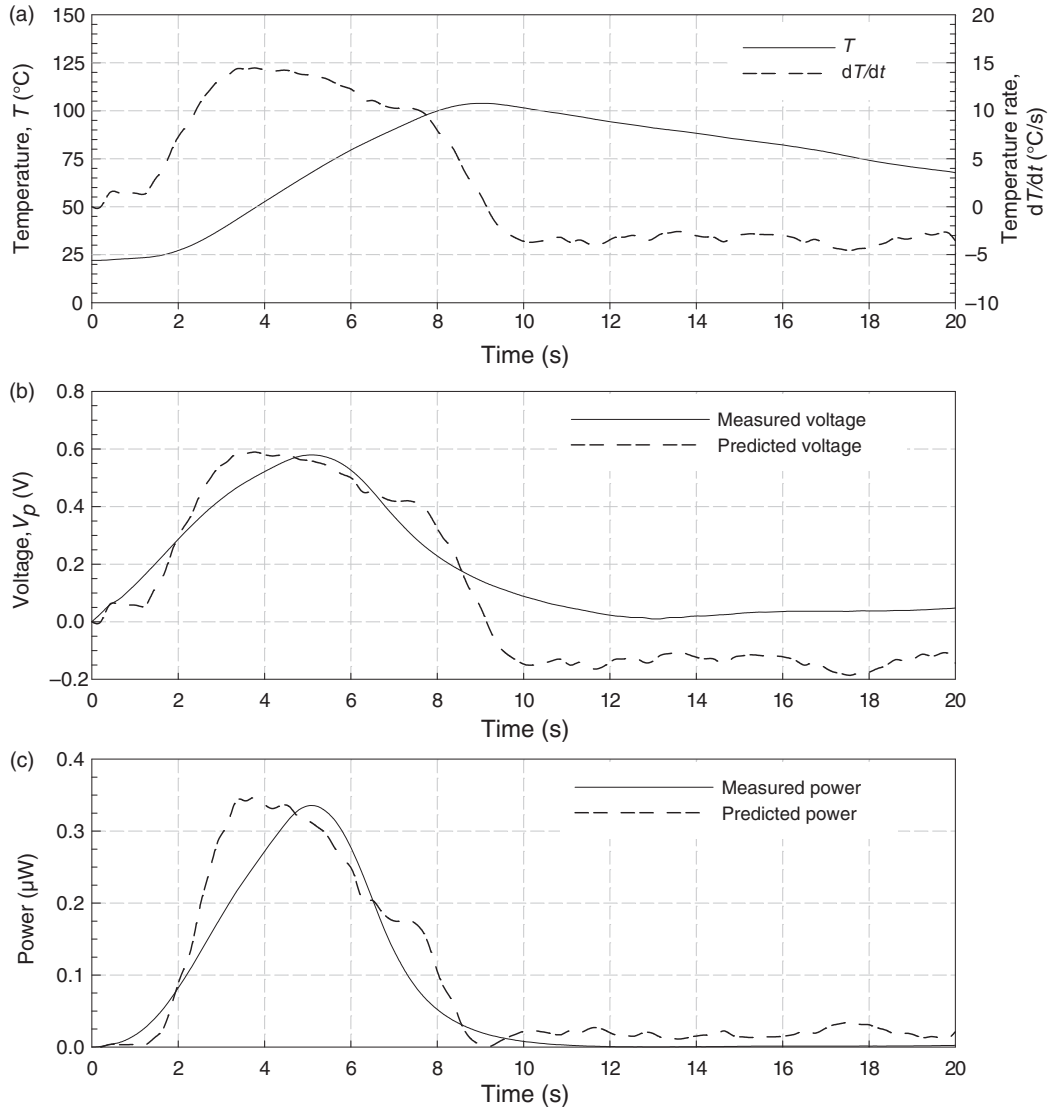

Figure 5. *Measured and predicted results of power generated by PMN-PT element: (a) temperature and temperature rate (dT/dt) vs time; (b) measured and predicted PMN-PT voltage vs time; and (c) measured and predicted power vs time.*

400 $\mu W/cm^2$ (Roundy and Wright, 2004). But since thermal gradients are readily available in many places, a combination of mechanical vibrations and heat could prove as a potential source of efficient energy harvesting.

It is important to note that there could be discrepancies in the results attributed to several factors. First, the temperature of the element was measured at a single point using the thermocouple sensor, and thus temperature may not have been uniform across the sample. Second, the temperature was measured on the backside resistance heater and was assumed to be the temperature of the sample. This assumption was made because relatively thin samples were used and the transient spatial temperature behavior across the thickness of the sample was ignored. In the case of PVDF, the material exhibited above average bonding characteristics at the interface between the heater and sample, and this could have introduced some error in the measurements.

To study the potential of using other pyroelectric materials for power generation, the model given by Equation (4) combined with the measured temperature profiles shown in Figures 4(a), 5(a), and 6(a) were used to predict power generation of samples with different sizes other than the ones tested experimentally. The model was also used to make predictions for materials with higher pyroelectric coefficient than the ones tested to further illustrate the potential that larger pyroelectric coefficients enhance the power generation. In particular, thin-film PST with pyroelectric coefficient $p' = 6000\,\mu C/m^2/K$ (Watton and Todd, 1991; Todd et al., 1999) and lead magnesium niobate-lead titanate (PMN-PT) with $p' = 300$ to over $1000\,\mu C/m^2/K$ (Kumar et al., 2004; Sebald et al., 2008) were considered.

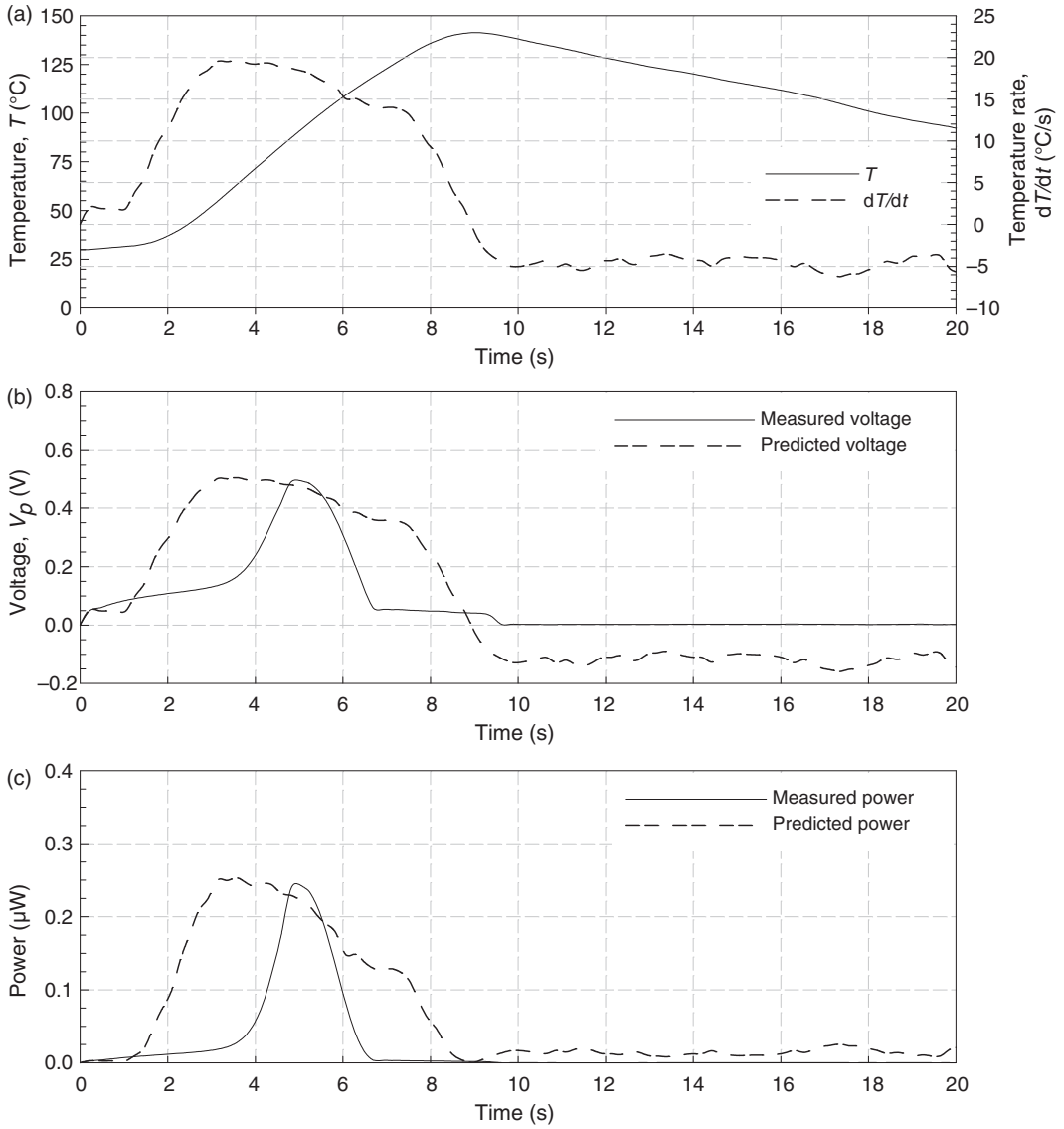

Figure 6. *Measured and predicted results of power generated by PVDF element: (a) temperature and temperature rate (*dT/dt*) vs time; (b) measured and predicted PVDF voltage vs time; and (c) measured and predicted power vs. time.*

Table 2. Measured and predicted result comparison.

	Peak voltage (V)			Peak power (μW)			Power density (μW/cm^2)		
Sample	**Measured**	**Predicted**	**Difference**	**Measured**	**Predicted**	**Difference**	**Measured**	**Predicted**	**Difference**
PZT-5A	0.53	0.58	9%	0.28	0.33	16%	0.20	0.23	14%
PMN-PT	0.57	0.59	4%	0.33	0.35	6%	0.33	0.36	9%
PVDF	0.49	0.53	8%	0.24	0.26	8%	0.12	0.13	8%

Figure 7 shows the peak power density as a function of area and pyroelectric coefficient. The area was varied between $1.44\,\text{cm}^2$ ($1.20\,\text{cm} \times 1.20\,\text{cm}$) to $3.63\,\text{cm}^2$ ($1.91\,\text{cm} \times 1.91\,\text{cm}$) and the capacitance was adjusted accordingly by assuming a constant electrode separation for a parallel-plate capacitor model. The pyroelectric coefficient was varied between $p' = 238\,\mu\text{C/m}^2\text{/K}$ and $p' = 6000\,\mu\text{C/m}^2\text{/K}$. The maximum power density calculated with these values was $340.875\,\mu\text{W/cm}^2$. The predicted result shows the potential for using thin-films with improved pyroelectric coefficient as well as maximizing the area of the energy-harvesting element. These results point out the importance of maximizing these variables for energy harvesting.

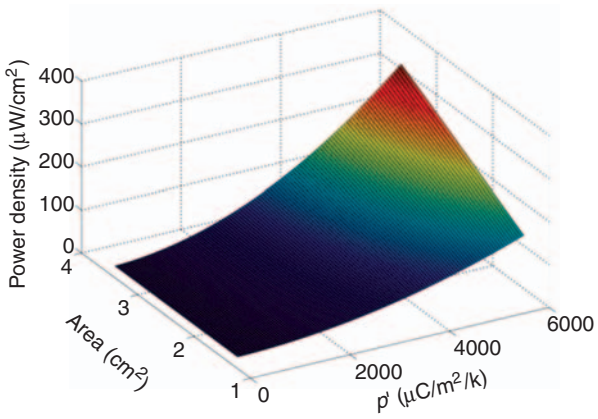

Figure 7. *Predicted peak power density as a function of pyroelectric coefficient and area based on same boundary conditions as the experiment on PZT-5A.*

CONCLUSIONS

The potential for energy harvesting through the pyroelectric effect was studied by using piezoelectric materials such as PZT-5A, PMN-PT, and PVDF. A model was developed to predict the power generation. Measured results were compared to predicted results, as shown in Table 2. The measured results were in good agreement with the predicted results for the three tested samples. The results were within 4%, 8% and 9% for PMN-PT, PVDF, and PZT-5A, respectively. Peak power densities were experimentally determined to be 0.33, 0.20, and 0.12 $\mu W/cm^2$, for PMN-PT, PVDF, and PZT-5A, respectively. Using the model it was predicted that a thin-film with large area and significantly higher pyroelectric coefficient can generate nearly three orders of magnitude improved peak power density under similar boundary conditions as the PZT-5A, PMN-PT, and PVDF samples.

ACKNOWLEDGMENTS

Authors would like to acknowledge the support of NextGen Aeronautics, specifically Shiv Joshi and Scott Bland, as well as the Air Force Research Laboratory. Authors also thank Andrew J. Fleming for making suggestions on the power measurement circuit.

REFERENCES

APC International, Ltd. 2002. *Piezoelectric Ceramics: Properties & Applications*, APC International, Mackeyville, PA, USA.

Bauer, S. 2006. "Piezo-, Pyro- and Ferroelectrics: Soft Transducer Materials for Electromechanical Energy Conversion," *IEEE Transactions on Dielectrics and Electrical Insulation*, 13:953–962.

Borisenok, V.A., Koshelev, A.S. and Novitsky, E.Z. 1996. "Pyroelectric Materials for Converters of Pulsed Ionizing Radiation Energy into Electric Power," *Bulletin of the Russian Academy of Sciences, Physics*, 60:1660–1662.

Cuadras, A., Gasulla, M., Ghisla, A. and Ferrari, V. 2006. "Energy Harvesting from PZT Pyroelectric Cells," In: Instrumentation and Measurement Technology Conference, Sorento, Italy, pp. 1688-1672.

Guyomar, D., Sebald, G., Lefeuvre, E. and Khodayari, A. 2009. "Toward Heat Energy Harvesting Using Pyroelectric Material," *Journal of Intelligent Material Systems and Structures*, 20:265–271.

Kumar, P., Sharma, S., Thakur, O.P., Prakash, C. and Goel, T.C. 2004. "Dielectric, Piezoelectric and Pyroelectric Properties of PMN-PT (68:32) System," *Ceramics International*, 30:585–589.

Lam, S.K., Wong, Y.W., Tai, L.S., Poon, Y.M. and Shin, F.G. 2004. "Dielectric and Pyroelectric Properties of Lead Zirconate Titanate/Polyurethane Composites," *Journal of Applied Physics*, 96:3896–3899.

Lu, F., Lee, H.P. and Lim, S.P. 2004. "Modeling and Analysis of Micro Piezoelectric Power Generators for Micro-electromechanical-System Applications," *Smart Materials and Structures*, 13:57–63.

Malmonge, L.F., Malmonge, J.A. and Sakamoto, W.K. 2003. "Study of pyroelectric activity of PZT/ PVDF-HFP composite," *Materials Research*, 6:469–472.

Mossi, K.M., Green, C., Qunaies, Z. and Hughes, E. 2005. "Harvesting Energy Using a Thin Unimorph Prestressed Bender: Geometrical Effects," *Journal of Intelligent Material Systems and Structures*, 16:249–261.

Nersessian, N., Carman, G. P. and Radousky, H. B. 2008. "Energy harvesting using a thermoelectric material," United States Patent 7397169.

Paradiso, J.A. and Starner, T. 2005. "Energy Scavenging for Mobile and Wireless Electronics," *Pervasive Computing,* 4:18–27.

Roundy, S., Wright, P. and Rabaey, J. 2003. "A Study of Low Level Vibrations as a Power Source for Wireless Sensor Nodes," *Computer Communication*, 26:1131–1144.

Roundy, S. and Wright, P. 2004. "A Piezoelectric Vibration Based Generator for Wireless Electronics," *Smart Materials and Structures*, 13:1131–1142.

Rowe, D.M. 1995. *CRC Handbook of Thermoelectrics*, CRC Press, Boca Raton, FL.

Rowe, D.M. 1999. "Thermoelectric, an Environmentally-friendly Source of Electrical Power," *Renewable Energy*, 16(1):1251.

Sebald, G., Lefeuvre, E. and Guyomar, D. 2008. "Pyroelectric Energy Conversion: Optimization Principles," *IEEE Transactions on Ultransonics, Ferroelectrics and Frequency Control*, 55:538–551.

Sodano, H.A., Inman, D.J. and Park, G. 2004. "A Review of Power Harvesting from Vibration Using Piezoelectric Materials," *The Shock and Vibration Digest*, 36:197–205.

Sodano, H.A., Simmer, G.E., Dereux, R. and Inman, D.J. 2007. "Recharging Batteries Using Energy Harvested from Thermal Gradients," *Journal of Intelligent Material Systems and Structures*, 18:3–10.

Teyssedre, G., Bernes, A. and Lacabanne, C. 1995. "Cooperative Movements Associated with the Curie Transition in P(VDF-TrFE) Copolymers," *Journal of Polymer Science*, 33:879–890.

Todd, M.A., Donohue, P.P., Jones, J.C., Wallis, D.J., Slatter, M.J., Harper, M.A. and Watton, R. 1999. "Deposition and Annealing of Lead Scandium Tantalate Thin Films for High Performance Thermal Detector Arrays," *Integrated Ferroelectrics*, 25:113–123.

Ujihara, M., Carman, G.P. and Lee, D.G. 2007. "Thermal Energy Harvesting Device Using Ferromagnetic Materials," *Applied Physics Letters*, 91:093508.

Watton, R. and Todd, M.A. 1991. "Induced Pyroelectricity in Sputtered Lead Scandium Tantalite Films and their Merit for IR Detector Arrays," *Ferrooelectrics*, 118:279–295.

Whatmore, R.W. 1986. "Pyroelectric Devices and Materials," *Reports on Progress in Physics*, 49:1335–1386.

Wu, C. 1996. "Analysis of Waste-heat Thermoelectric Power Generators," *Applied Thermal Engineering*, 16:63.